Inner gorges incision history: A proxy for deglaciation? Insights from Cosmic Ray Exposure dating (10Be and 36Cl) of river-polished surfaces (Tinée River, SW Alps, France)

Y. Rolland, C. Petit, M Saillard, Regis Braucher, Didier Bourlès, R. Darnault, D Cassol, A.S.T.E.R. Team

Earth and Planetary Science Letters 457 (2017) 271–281

Contents lists available at ScienceDirect

Earth and Planetary Science Letters

www.elsevier.com/locate/epsl

Inner gorges incision history: A proxy for deglaciation? Insights from Cosmic Ray Exposure dating (^{10}Be and ^{36}Cl) of river-polished surfaces (Tinée River, SW Alps, France)

Y. Rolland [a,*], C. Petit [a], M. Saillard [a], R. Braucher [b], D. Bourlès [b], R. Darnault [c], D. Cassol [a], ASTER Team [b,1]

[a] Université Côte d'Azur, CNRS, OCA, IRD, Géoazur, France
[b] Aix-Marseille Université, CNRS-IRD-Collège de France, UM 34 CEREGE, Technopôle de l'Environnement Arbois-Méditerranée, BP80, 13545 Aix-en-Provence, France
[c] IFP Energies Nouvelles, 1 et 4 avenue de Bois-Préau, 92852 Rueil-Malmaison, France

ARTICLE INFO

Article history:
Received 3 March 2016
Received in revised form 4 October 2016
Accepted 6 October 2016
Available online 31 October 2016
Editor: A. Yin

Keywords:
river gorges
incision
CRE ^{10}Be and ^{36}Cl dating
river polished surfaces

ABSTRACT

^{10}Be and ^{36}Cl Cosmic Ray Exposure (CRE) dating performed on river polished surfaces of river gorges in a mountain-to-sea river system in the French SW Alps highlights transient erosional events involving incision rates >10 mm a^{-1}. These events took place during the last two major deglaciation phases following (1) the Last Glacial Maximum (LGM) at 16–14 ka, (2) the Younger Dryas at 8–11 ka, and during the warm and humid Holocene climatic optimum at 4–5 ka. These periods of high incision rates (3–>30 mm a^{-1}) alternated with periods of low incision rates (<1 mm a^{-1}), which probably correspond to a long-term equilibrium between incision and relative uplift. The Alpine river staircase shape profiles evidence local and transient responses that are ascribed to cumulate disequilibrium after the long-time-spanned glaciations. After each glaciation, rivers rush down to get closer to their equilibrium profile. Incision is amplified both by the sediment discharge due to the erosion of moraines and by landslides triggered by the glacier retreat.

1. Introduction

Mountain rivers are key geomorphological features to understand the evolution of landscapes (Pratt et al., 2002; Brocard et al., 2003). The morphology of these features is directly linked to geological and geomorphological processes affecting mountain ranges (tectonic activity, mass wasting events and climate changes), and allows deciphering incision history over the Late Quaternary (e.g., Valla et al., 2011). In particular, inner gorges, which are secondary steep canyons dug inside a previously larger valley, are expressions of high and recent incision rates (>10 mm a^{-1}) and can be related to various factors such as active tectonics, climate change or modern agriculture (Koppes and Montgomery, 2009). However, the origin of inner gorges remains disputed. Several factors can lead to the formation of gorges, including localized uplift or base-level fall (Kelsey, 1988; Ouimet et al., 2008). In the case of the European Alps, which bear moderate uplift rates, two controversial hypotheses have been proposed:

(i) The gorges could mainly be dug during inter-glacial stages due to regained alluvial incision (e.g., Penk and Brückner, 1909; McEwen et al., 2002; Brocard et al., 2003; Schlunegger and Hinderer, 2003; Meigs et al., 2006; Valla et al., 2010), or,

(ii) they could mostly be formed below the glaciers by sub-glacial stream incision, and exposed as a whole after the glacial recession (Montgomery and Korup, 2011; Dixon, 2011).

Gorges are well suited to quantify incision rates at the scale of several 10^4 years applying Cosmic Ray Exposure (CRE) dating on vertical exposed polished surfaces (Valla et al., 2010; Saillard et al., 2014). CRE ages obtained from in situ-produced ^{10}Be concentration measurements suggest that some Alpine gorges result from a long-term incision rate of ~0.8 mm a^{-1}, but were rapidly incised (>10 mm a^{-1}) after the last glacial maximum (LGM) (Brocard et al., 2003; Valla et al., 2010). However, Dixon (2011) explained that the interpretation of ^{10}Be CRE ages in inner gorges can be complicated by the presence of a glacier cap: gorges may be carved beneath glaciers, preventing the accumulation of ^{10}Be during the initial stage of incision, before the glacier receded. Moreover, if the valleys were carved over successive inter-

* Corresponding author.
E-mail address: yrolland@unice.fr (Y. Rolland).
[1] Members of the Team are: M. Arnold, G. Aumaître, K. Keddadouche.

http://dx.doi.org/10.1016/j.epsl.2016.10.007
0012-821X/

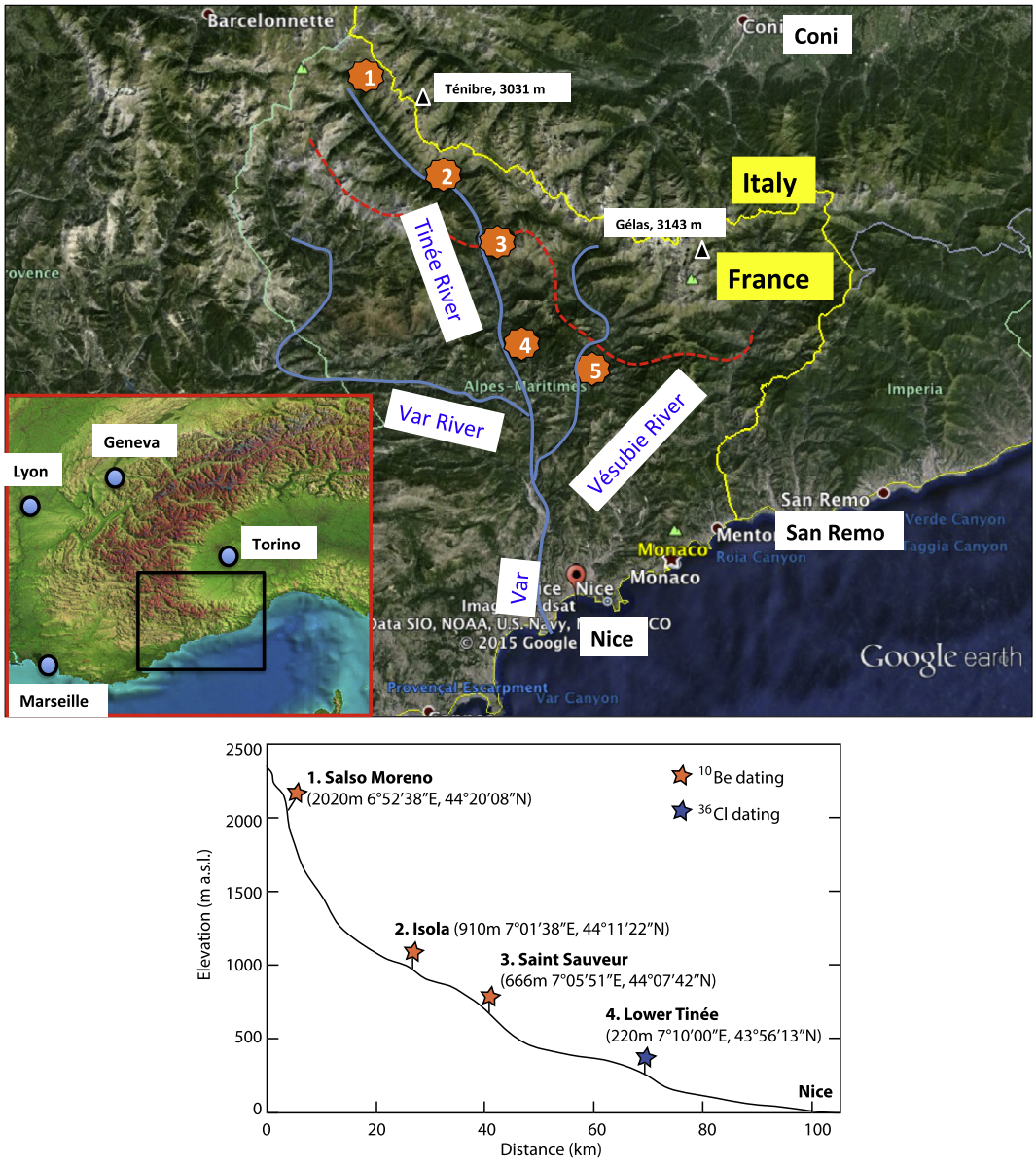

Fig. 1. A. Localization of study area, the Tinée River in SW Alps (France), and positions of the dated inner gorges: 1, Salso Moreno; 2, Isola; 3, Saint-Sauveur–de Tinée; 4: Lower Tinée. The profile 5, in the Vésubie River was investigated by Saillard et al. (2014). Red stripped line: Maximal advance of glaciers during the LGM, after Darnault et al. (2012) and Brisset et al. (2015). B. Tinée River longitudinal profile, with locations of studied inner gorges investigated by the cosmogenic nuclide ^{10}Be and ^{36}Cl dating methods in this study. (For interpretation of the references to color in this figure, the reader is referred to the web version of this article.)

glacial periods, evidence of previous exposures would be reset by subsequent denudation stages. Furthermore, temporal oscillations of valley aggradation and degradation can occur in response to climate-driven changes such as runoff intensity (Pratt et al., 2002). Then, interpreting CRE ages can also be complicated by episodic shielding by sediments during stages of valley aggradation. Other shielding effects, like landslides, which lead to natural dams in the river, may also result in the gorge walls to be hidden from cosmic rays (Pratt et al., 2002).

In this study, we use ^{10}Be and ^{36}Cl CRE dating of well-preserved river polished surfaces to constrain incision rates along several gorge profiles along the Tinée River. The Tinée River is a small-size (100 km-long) river system, flowing down from a 3000-m high mountain range to the sea base-level after merging with the Var River (Fig. 1), which is the main stream. While its source area has been under the influence of glaciations, its lower part is under a permanent alluvial regime, which allows addressing the question of the relative influences of glacial and of fluvial regimes in the shaping of inner gorges.

Three ^{10}Be CRE age profiles have been collected in the crystalline basement of the Argentera–Mercantour Massif, and one ^{36}Cl profile was collected in the limestones of the Mesozoic sedimentary cover upstream the junction of Var and Tinée Rivers. This latter will be compared to the one documented in the Lower Vésubie Valley at a similar latitude by Saillard et al. (2014). These new data provide a chronology of inner-gorges formation along the Tinée River since the Last Glacial Maximum (LGM). Based on these data origin and dynamics of fluvial incision in the South-western European Alps are discussed.

2. Area description, geological setting and previous works

The Tinée River runs across the Mercantour Range in the north, which culminates at 3200 m, and branches to the Var River, which flows into the Mediterranean Sea west of the city of Nice (Fig. 1).

Table 1
^{10}Be sample characteristics and exposure ages from the Tinée River polished surfaces.

Sample ID	Height from river	Quartz (g)	Thickness (cm)	Shielding factor[a]	^{10}Be/^{9}Be	± (%)	Be carrier (at)	[^{10}Be] (at g^{-1})[b]	^{10}Be age (ka) global PR[c]	± (1σ)
Salso Moreno (Profile 1): 6°52′38″E, 44°20′08″N, 2020 m										
SM1	36	82.0	5	0.51	4.37E−13	10	2.04722E+19	108,666	10.7	1.0
SM2	31	58.7	6	0.51	1.46E−13	9	2.03994E+19	50,004	4.95	0.45
SM3	28.6	20.5	4	0.50	6.87E−14	9	2.04725E+19	65,258	6.57	0.59
SM4	26	64.4	5	0.50	4.89E−14	25	2.04883E+19	14,941	1.51	0.39
SM5	22	42.3	4	0.48	2.35E−14	14	2.03853E+19	10,401	1.10	0.16
SM6	18	61.8	5	0.46	3.17E−14	17	2.0268E+19	9,771	1.08	0.18
SM7	12	47.8	6	0.44	2.11E−14	22	2.02802E+19	8,165	0.95	0.21
SM8	7	70.4	5	0.41	8.46E−15	27	2.1602E+19	2,016	0.25	0.67
SM9	4	43.6	4	0.40	6.38E−15	17	2.05106E+19	2,113	0.27	0.47
Isola (Profile 2): 7°01′35″E, 44°11′22″N, 910 m										
CLAP68	18.0	18.9	16	0.86	2.49E−14	29	2.04644E+19	23438	2.87	0.83
ISO-13-1	18.5	22.9	18	0.86	1.24E−14	22	2.03168E+19	8,128	0.92	0.20
ISO-13-2	20.3	22.1	15	0.86	2.59E−14	15	2.04341E+19	21,048	2.37	3.49
ISO-13-3	24.8	15.3	17	0.86	2.98E−14	8	2.04543E+19	35,579	3.99	0.33
ISO-13-7	26.9	22.7	15	0.86	2.43E−14	11	2.04725E+19	20,076	2.95	0.31
ISO-13-4	31.0	21.5	16	0.86	3.83E−14	11	2.04563E+19	26,392	2.24	0.24
ISO-13-5	33.9	23.0	10	0.86	3.92E−14	10	2.03471E+19	31,073	3.46	0.37
ISO-13-6	40.4	22.7	9	0.86	3.25E−14	11	2.04745E+19	32,499	3.60	0.36
CLAP70	46.0	20.8	11	0.86	5.86E−14	10	2.02461E+19	53,883	6.57	0.66
CLAP76	149.0	4.2	13	0.86	2.54E−14	14	2.05149E+19	107,911	19.0	2.7
Saint-Sauveur-Sur-Tinée (Profile 3): 7°05'52"E, 44°07'42"N, 666 m										
Ti-15-1	38.45	14.4	6	0.61	6.93E−14	10	2.01429E+19	94672	22.8	2.2
Ti-15-2	35.3	14.4	3	0.61	5.95E−14	7	2.05755E+19	82892	19.1	1.3
Ti-15-3	32.6	9.8	5	0.61	6.56E−14	9	2.04522E+19	133837	32.0	2.9
Ti-15-4	28.7	14.7	2	0.61	5.79E−14	12	2.04865E+19	78284	17.8	2.2
Ti-15-5	26.1	12.8	3	0.61	5.22E−14	7	2.05815E+19	81631	18.9	1.3
Ti-15-11	21.8	12.3	2	0.61	5.12E−14	6	2.05553E+19	83083	19.0	1.1
Ti-15-6B	18.8	19.8	2	0.61	8.04E−14	5	2.06402E+19	82142	23.4	1.1
Ti-15-7	15.6	11.0	5	0.61	4.74E−14	5	2.04987E+19	85287	19.6	1.0
Ti-15-8	12.9	9.8	3	0.61	4.41E−14	8	2.04138E+19	88366	21.4	1.7
Ti-15-9	9.5	10.7	13	0.61	1.31E−14	21	2.0527E+19	22139	5.17	1.11
Ti-15-10	0.5	15.7	1.5	0.61	1.11E−14	16	2.05856E+19	12481	3.43	0.56

[a] Azimuths and angular elevations (0–90°) to calculate the shielding factor were recorded using a compass and clinometer (see Analytical Procedures section).
[b] All samples measured at the French AMS national facility 'ASTER'. AMS results are standardized to NIST_27900. ^{10}Be/^{9}Be ratios were corrected for a process blank value of (1.1 ± 0.4) 10–15 for profile 1, (9.9 ± 2.6) 10–15 for profile 2, (9.5 ± 2.3) 10–16 for profile 3.
[c] See the analytical procedures (section 3) for CRE age calculations. Used density is 2.7.

The Mercantour high topography is driven by a current transpressive tectonic context (e.g., Bauve et al., 2014; Jourdon et al., 2014; see Fig. 1 in suppl. Mat. 1 for geology). Long-term exhumation rate estimates derived from thermochronology in the Mercantour are of 0.8–1 mm a^{-1} since 22 Ma (Sanchez et al., 2011). Apatite Fission Tracks and U–Th/He studies document increased denudation rates since 5 Ma at the scale of the whole Alpine range, which is interpreted as the onset of efficient glacier-driven erosion (Vernon et al., 2008). In addition, high uplift rates of 1–2 mm a^{-1} and almost null horizontal velocities have been obtained by GPS measurements (Serpelloni et al., 2013) in the higher parts of the Alps, which suggests an influence of erosion and isostasy in the construction of Alpine topography (e.g., Herman and Champagnac, 2016). In particular, the uppermost part of the Tinée Valley has been extensively shaped by recent Quaternary glaciations (Sanchez et al., 2010; Darnault et al., 2012). These studies indicate mainly two major glacier recessions: 1) at the Late-glacial period (16–15 ka) which directly followed the last Glacial Maximum (LGM), and 2) at the end of the Younger Dryas (~11 ka), like in the north Argentera slope and High Durance Valley area (Federici et al., 2008; Cossart et al., 2010) and in the Northern Alps (Ivy-Ochs et al., 2009). Following these deglaciation stages, some important landslides were triggered, amongst which 'La Clapiere' and 'Le Pra' Landslides (Fig. 1). Three phases of landslide activity are evidenced for La Clapière Landslide at 10 ka, 7 ka and 2 ka, while Le Pra landslide was triggered at around 5 ka (Sanchez et al., 2010). Numerical modelling and combined CRE dating suggest landslide activity is a consequence of slopes steepening due to river incision (Bouissou et al., 2012). Pioneering CRE dating of polished river bedrock in another nearby downstream tributary of the Var River (the Vésubie River) was undertaken by Saillard et al. (2014) using ^{36}Cl CRE dating on calcite (Fig. 1). In this study, a ~25 m high vertical profile gave CRE ages ranging from 3 to 14 ka, with a mean incision rate of 2.2 mm a^{-1}. Two peaks of increased incision were recognized at 4–5 ka and 11–12 ka, reaching rates of 2 and 4–5 mm a^{-1}, respectively, separated by a period experiencing a lower incision rate (~1 mm a^{-1}). These variations were interpreted to reflect increases in the water runoff due to climate change during the Holocene climatic optimum and the Younger Dryas deglaciation, respectively.

3. CRE dating: sampling strategy and analytical procedures

We aimed at collecting perfectly fresh river-polished surfaces along the Tinée River stream, to avoid effects of potential surface rejuvenation. The sampling sites were selected to document incision history at regular intervals from the seacoast up to the mountain range, where fresh polished outcrops could be unambiguously identified (see Figs. 4–6 in suppl. mat. 1). Samples were collected along the cliff using a hammer and chisel. Their latitude, elevation, position along the profile and exposure geometry were precisely determined in the field (Tables 1–2). Bedrock samples for ^{36}Cl CRE dating consist of pure limestone (compositions have been measured by ICPMS for all samples, see suppl. mat. 2), and gneiss (mica–feldspar–quartz) for ^{10}Be CRE dating. For details on methods, calculations and related errors, the reader is referred to Braucher et al. (2011), while the approach is briefly summarized below.

Table 2
^{36}Cl sample characteristics and exposure ages from the Tinée River polished surfaces.*

Sample ID	Height from river	^{35}Cl (ppm)	Shielding factor[a]	[^{36}Cl] (at g^{-1})[b]	± (1σ)	^{36}Cl age (ka)	± (1σ)
Lower Tinée (Profile 4): 7°10′00″, 43°56′13″, 300 m							
Ti-13-12	25.8	47.92	0.61	273602	5,882	16.68	0.36
Ti-13-13	24.15	49.86	0.62	218729	4,577	13.09	0.27
Ti-13-14	22.8	45.99	0.61	222029	4,537	13.54	0.28
Ti-13-15	20.15	38.34	0.61	209408	4,145	13.08	0.26
Ti-13-01	17.75	37.15	0.62	230889	4,366	14.35	0.27
Ti-13-02	16.5	36.96	0.62	206645	4,011	12.81	0.25
Ti-13-04	13.5	45.38	0.62	216616	4,507	13.56	0.28
Ti-13-05	11.4	41.45	0.61	212695	4,395	13.33	0.28
Ti-13-06	9.85	45.05	0.62	204344	4,873	12.30	0.29
Ti-13-07	8	37.85	0.61	133351	3,194	8.33	0.20
Ti-13-08	7.15	35.26	0.61	126436	3,133	8.09	0.20
Ti-13-09	5.05	37.89	0.60	142947	3,330	9.09	0.21
Ti-13-10	2.3	43.11	0.59	136159	3,389	8.64	0.21
Ti-13-11	0.7	53.27	0.56	131351	3,554	8.73	0.24

Sample thickness is 5 cm.

[a] Azimuths and angular elevations (0–90°) to calculate the shielding factor were recorded using a compass and clinometer (see Analytical Procedures section).

[b] All samples measured at the ASTER facility. AMS results are standardized to KNSTD1600. ^{36}Cl/^{37}Cl ratios were corrected for a process blank value of 6.4×10^{-12}.

* To compare the ^{36}Cl exposure ages presented in this paper with ages issued from different dating methods a 4.76% uncertainty related to the spallation (Braucher et al., 2011). Production rate has to be added to the internal uncertainties. Spallation production rate is 42 ± 2.0 atoms of ^{36}Cl g^{-1} of Ca a^{-1}.

3.1. ^{36}Cl dating

The samples were crushed, sieved and chemically prepared at the French Cosmogenic Nuclides National Laboratory (LN2C; CEREGE, Aix-en-Provence) to precipitate AgCl following the procedure fully described in Schimmelpfennig et al. (2009). Their ^{36}Cl and Cl concentrations were determined by isotope dilution Accelerator Mass Spectrometry at the French AMS national facility ASTER (CEREGE, Aix-en-Provence) and were both normalized to a ^{36}Cl standard prepared by K. Nishiizumi: KNSTD1600 with a given ^{36}Cl/^{35}Cl-value of $(6.40 \pm 0.06) \times 10^{-12}$. The decay constant of $2.303 \pm 0.016 \times 10^{-6}$ a^{-1} used corresponds to a ^{36}Cl half-life ($T_{1/2}$) of 3.014×10^5 years. All the analytical and chemical data are presented with respect to the recommendations of Dunai and Stuart (2009). Analytical uncertainties include the counting statistics, machine stability and blanks correction (^{36}Cl/^{35}Cl blank ratios are 0.75 and 3.87×10^{-15}). Blank corrections represent between 0.6 and 6.7% of the sample concentrations. Cl concentrations of the samples range from 15 to 32 ppm.

The estimation of ^{36}Cl production rate requires 1) the analysis of samples' chemical composition (i.e. relative abundance of target elements) and 2) the intensity of the incoming cosmogenic flux. (1) The chemical composition of all samples was analyzed by ICP-AES and ICP-MS at the CRPG-SARM facility (Nancy, France) in order to ensure that the chemical composition of limestone was homogeneous, which appears to be the case (data are shown in Suppl. Mat. 2). The data show limited variability of Li (1.1–2.5 ppm), Al_2O_3 (0.05–0.45 wt%) and MgO (0.36–0.52 wt%) contents. (2) All the contributions from the various ^{36}Cl production mechanisms using these relevant parameters were then taken into account to determine each sample specific production rate (Schimmelpfennig et al., 2009). The in situ-produced ^{36}Cl production rate also depends on the incoming cosmic ray flux that varies with the Earth magnetic field, with the latitude and elevation of the study area and with the amount of topographic obstruction around the sample, the latter being generally the most important factor to take into account to obtain an accurate age estimate (Gosse and Phillips, 2001). Temporal geomagnetic field variations are negligible at these latitudes for ages >10 ka, and may induce 5% overestimation of production for ages <10 ka (e.g., Dunai, 2001), so they will have little or no effect on incision estimates and their temporal pattern. Thus, over the period considered, the latitudinal and altitudinal scaling were determined at a constant geomagnetic field (Stone, 2000). The elementary ^{36}Cl production rate from spallation of calcium at sea level and high latitude used is 42 ± 2.0 atoms of ^{36}Cl.gram^{-1} of Ca.a^{-1} as established at a site less than a few hundreds of km away from the sampling site (Braucher et al., 2011). Calibrated at a site for which latitude, elevation, and exposure duration are similar to those of the sampling site (i.e., La Ciotat at an altitude of 300 m), this "local" production rate significantly reduces the uncertainties linked to the scaling processes. The exposure ages were finally calculated according to Schimmelpfennig et al. (2009), with modified muons values based on Braucher et al. (2011).

3.2. ^{10}Be dating

For this study, the chemical treatment of samples and the AMS measurements were carried out at the "Laboratoire National des Nucléides Cosmogéniques (LN2C)" (CEREGE, Aix-en-Provence). Crushed rocks were sieved and magnetic grains were discarded using a magnetic separator. Pure quartz was obtained from the non-magnetic 250–800 µm fraction by repeated H_2SiF_6–HCl etching; atmospheric ^{10}Be was subsequently eliminated by sequential dissolutions with diluted HF. After addition in each sample of ~100 µl of an in-house 3.10^{-3} g/g ^{9}Be carrier solution prepared from deep-mined phenakite (Merchel et al., 2008), residual grains were dissolved in a strong HF solution. Upon complete evaporation of SiF_6, remaining solutions were purified and beryllium was separated by anion and cation exchange columns, respectively, after which alkaline precipitations allowed to extract Be. BeO targets were prepared for measurement at the French National Accelerator Mass Spectrometry facility, ASTER, located at CEREGE in Aix en Provence. The obtained ^{10}Be/^{9}Be ratios were corrected for procedural blanks and calibrated against the National Institute of Standards and Technology standard reference material 4325 by using an assigned value of $2.79 \pm 0.03 \times 10^{-11}$ and using a ^{10}Be half-life of $(1.387 \pm 0.012) \times 10^6$ years (Korschinek et al., 2010; Chmeleff et al., 2010). Further, to calculate the ages from the measured concentrations, the following equation was used:

$$C_{(\chi,\varepsilon,t)} = C_0 e^{-\lambda t} + \frac{P_{spal.}}{\lambda} e^{-\frac{\chi}{\Lambda_n}} \left[1 - e^{-t\lambda}\right] + \frac{P_{\mu s}}{\lambda} e^{-\frac{\chi}{\Lambda_{\mu s}}} \left[1 - e^{-t\lambda}\right] + \frac{P_{\mu f}}{\lambda} e^{-\frac{\chi}{\Lambda_{\mu f}}} \left[1 - e^{-t\lambda}\right]$$

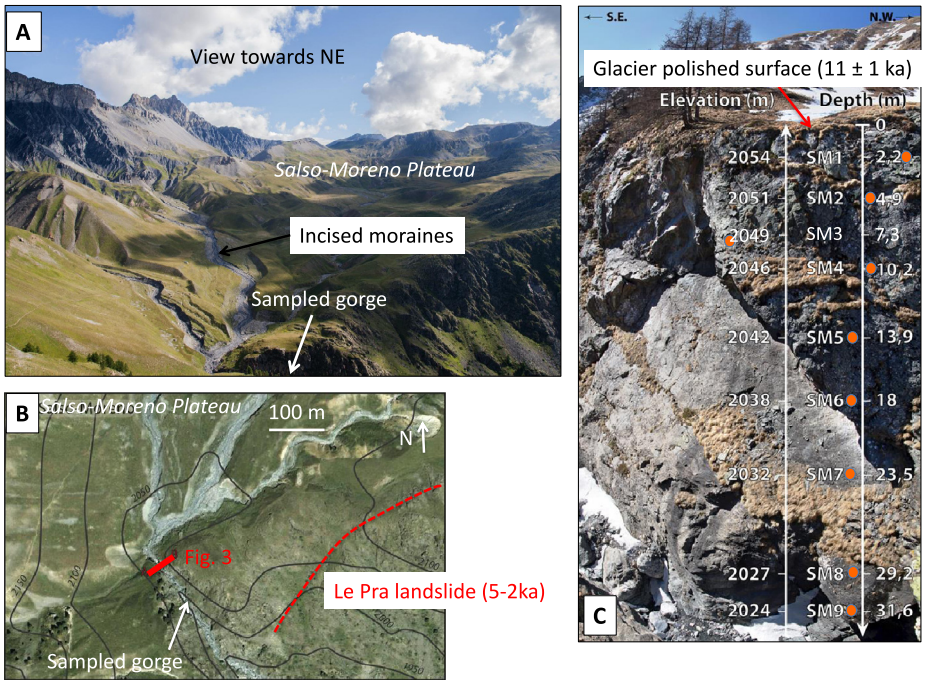

Fig. 2. A, General view of the Salso-Moreno Plateau upstream Tinée Valley. B, aerial photograph of the Salso-Moreno Gorge at the rim of the flat glacial plateau. C, photograph of the sampled vertical cliff in the gorge. For a detailed description of the neighboring "Le Pra" landslide, the reader is referred to Sanchez et al. (2010).

where $C_{(\chi,\varepsilon,t)}$ is the ^{10}Be concentration as a function of depth χ ($g\,cm^{-2}$), erosion ε ($g\,cm^{-2}\,yr^{-1}$) and t the exposure time (yr). C_0 is the ^{10}Be inherited concentration prior to exposure at the surface. Λ_n, $\Lambda_{\mu s}$ and $\Lambda_{\mu f}$ are the effective apparent attenuation length ($g\,cm^{-2}$) for neutrons, slow muons and fast muons, respectively. P_{spal}, $P_{\mu s}$ and $P_{\mu f}$ are the relative spallogenic, slow and fast, respectively. P_{spal}, $P_{\mu s}$ and $P_{\mu f}$ are the relative spallogenic, slow and fast muons production rates. All calculations were performed using attenuation lengths of 150, 1500 and 4320 $g\,cm^{-2}$. These values are based on field-calibrated measurements (Braucher et al., 2011). A modern spallogenic production rate at sea-level and high latitude of 4.02 ± 0.20 atoms $g^{-1}\,yr^{-1}$, computed for internal consistency from the data of Stone (2000) according to the conclusions of the published study on absolute calibration of ^{10}Be AMS standards (Nishiizumi et al., 2007), was used. This sea-level and high latitude production rate has then been scaled for the sampling altitudes and latitudes using the scaling factors proposed by Stone (2000). Analytical uncertainties (reported as 1σ) include a conservative 0.5% uncertainty based on long-term measurements of standards, a 1σ statistical error on counted ^{10}Be events, and the uncertainty associated with the chemical and analytical blank correction. To compare the ^{10}Be CRE ages with absolute ages, one has to add an additional ~5% uncertainty for production rate.

3.3. Shielding estimates

The surface production rates were corrected for local slope and topographic shielding due to surrounding morphologies (Dunne et al., 1999). In our case, the topographic shielding was particularly important because the samples were collected on an almost vertical surface, which means that up to 50% of the incoming ray flux was blocked by the topography in the immediate vicinity of the samples. In order to insure a correct estimate of the topographic shielding, we have measured the cliff slope. Besides the cliff itself, the shielding effect of the surrounding topography was measured with a compass as the height (in degrees) of the horizon with respect to the horizontal. The topographic shielding factor S_f is then as follows:

$$S_f = \int_{\Phi=0}^{2\pi} \int_{\theta=\theta_h}^{\pi/2} \sin^{2.3}\theta \cos\theta d\theta d\Phi$$

Where θ is the angle of incidence of cosmic rays measured from the horizontal, θ_h is the angle of topographic obstruction, Φ is the azimuth. Shielding factors range from 0.40 for the most shielded samples to 0.86 for the most exposed ones (Tables 1–2). Measurement error of the topographic obstruction of about 5° will induce shielding factor estimate uncertainties ranging from less than 0.4% (for a low dipping topography) to at most 5% (for large topographic angles). Moreover, the shielding between sampled points varies only with the local dip of the cliff (i.e., on an azimuth aperture of less than 180°). Consequently, such shielding factor estimate errors will introduce a systematic bias, which will affect absolute age values but will have a very limited effect on age differences, hence on the incision rate estimates.

3.4. Inherited component

Because the sampled bedrock is highly shielded and deep beneath from the overlying surface topography, the inherited component can be neglected in most cases. We tested the contribution of the inherited component in the Salso Moreno profile, which is dug into a flat glacier polished surface (Fig. 2). This profile has potentially the highest inherited contribution in all the analyzed profiles because the other profiles are in the lower part of valleys at the base of slopes >1000 m high.

The results of ^{10}Be analysis on the Salso Moreno profile are displayed on Suppl. Mat. 3, where they are compared to ^{10}Be inheritance concentration profiles related to denudation rates ranging from 600 $m\,Ma^{-1}$ to 30 $m\,Ma^{-1}$. The ^{10}Be concentrations at depth are fitted by the 30 $m\,Ma^{-1}$ curve. However, taking into account the Apatite-He ages of 4–5 Ma obtained at the same place by Sanchez et al. (2011), the long-term incision rate estimate is of 600 $m\,Ma^{-1}$. Given the similarity of geological context with the Pelvoux Massif, in which millennial scale denudation rates have been quantified using the ^{10}Be method, and range

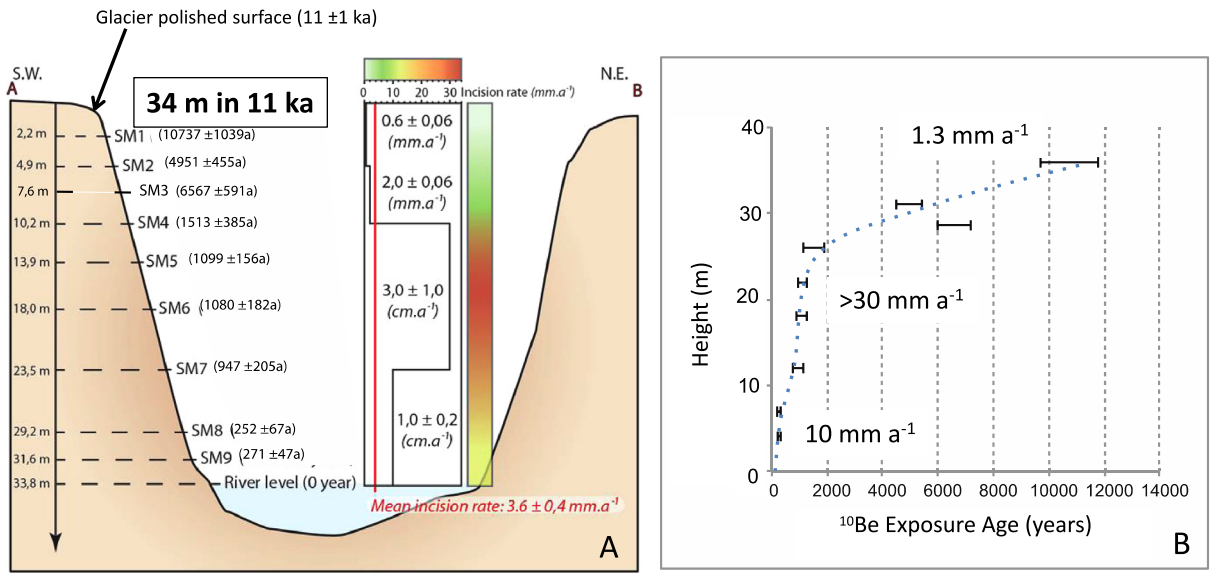

Fig. 3. A, Salso-Moreno Gorge profile and B, corresponding ^{10}Be ages.

from 270 ± 50 and 1070 ± 200 m Ma^{-1} (Delunel et al., 2010), the above 600 m Ma^{-1} estimate is most likely. Further, it is a lower estimate because the profile is in the axis of the glacier valley, and average estimates for denudation during the last major glaciations is about 2–3 mm a^{-1} in such zones (Delunel et al., 2010; Darnault et al., 2012). Therefore the apparent 'inherited profile' due to the logarithmic fit of the data is not ascribed to a significant inherited component. When a 600 m Ma^{-1} denudation rate is taken into account the inherited component is of 2% in the first 10 m, rising to 5% at 20 m, and finally 15% in the gorge lower part at 30 m. The part of inherited component increases with depth due to the very young age of the surface and thus the low corresponding amount of cosmonuclides produced by direct exposure. But considering the incision rate is maximal in the Salso Moreno profile, this 15% inherited contribution is a maximum value, largely within the error margin in the present example. In conclusion, the exposure ages are thus maximal ages, yielding to potentially underestimated incision rates. Given the reasons presented above, the age bias due to possible inherited ^{36}Cl or ^{10}Be is most likely negligible and anyway systematic; hence, it does not affect the incision rate estimates.

4. Results

The results of ^{10}Be and ^{36}Cl CRE dating are described below from upstream to downstream the Tinée River, and presented in Tables 1–2.

4.1. ^{10}Be CRE dating of the Salso-Moreno Gorge profile (profile 1)

The first dated gorge profile is located in the Salso-Moreno area (Fig. 1; Fig. 2A), at an elevation of 2020–2060 m. This site was chosen because of a well-exposed 35 m-deep gorge directly incised in the glacial rock-bar on the edge of a flat plateau, polished by glaciers during the Younger Dryas (Sanchez et al., 2011). This profile provides nine ^{10}Be CRE ages ranging from 10.7 ± 1.0 ka at the top to 0.27 ± 0.05 ka at the bottom of the gorge (Table 1; Fig. 3).

The ^{10}Be CRE age profile shows a decrease in ages down to the river bed, i.e. from sample SM1 to SM9, except for SM3 (Fig. 3), which is slightly older due to its lateral down-stream position. Incision started at the end of the Younger Dryas and continued until present with a mean incision rate of 3.6 ± 0.4 mm a^{-1} for this time period. The ^{10}Be CRE age profile highlights 3 progressive incision steps since the Younger Dryas with different incision rates (Fig. 3):

(1) The first incision step corresponds to samples located from the top of the gorge to a depth of 10.2 m. The samples are dated from 10.7 ± 1 to 1.5 ± 0.4 ka, which gives a mean incision rate of 1.3 mm a^{-1}.

(2) From 10.2 to 23.5 m depth, ^{10}Be CRE ages remain similar within uncertainty, with a slight decrease from 1.5 ± 0.4 ka to 0.9 ± 0.2 ka, and accordingly the incision rate increases to >30 mm a^{-1}.

(3) The two lower samples dated at 252 ± 67 and 271 ± 47 a, respectively, implying that the lower 10 m gorge have been incised in less than ∼1000 yrs at a rate of about 10 mm a^{-1}.

4.2. ^{10}Be dating of the Isola Gorge (profile 2)

The eleven ^{10}Be CRE ages obtained along the Isola Gorge polished surface (Fig. 1; Fig. 4) show an increase in ages from 1–2 ka at the base of profile (930 m) up to 6.5 ± 0.7 ka at the top of the first 25-m high scarp, and 19.0 ± 2.8 ka high up in the slope (1070 m). Taking into account the present-day elevation of the Tinée River (920 m), these ages give an incision rate of about 7.7 mm a^{-1} since about 20 ka. However, in the first 25-m high scarp from the base of the profile (Fig. 4B) most CRE ages range between 2239 and 3598 a, which suggests a very rapid incision event for this part of the scarp (25 m in about 1 ka).

4.3. ^{10}Be dating of the Saint Sauveur Gorge (profile 3)

The eleven ^{10}Be CRE ages obtained along the polished surface of the Saint-Sauveur–Sur-Tinée Gorge range between 3.1 ± 0.5 and 20.4 ± 2.0 ka, from the base to the top of profile, respectively (Fig. 5). Although these CRE ages lead to a mean incision rate of 2 mm a^{-1} since 20 ka, two age groups may be distinguished:

(i) From the top of cliff (40 m) to about 10 m, a first group of ages clusters at 18.1 ± 1.8 ka, the sole outlier at 28 ka being not considered as geologically meaningful.
(ii) In the lower part of section (<10 m), a second group of two ages at 3–4.6 ka is observed.

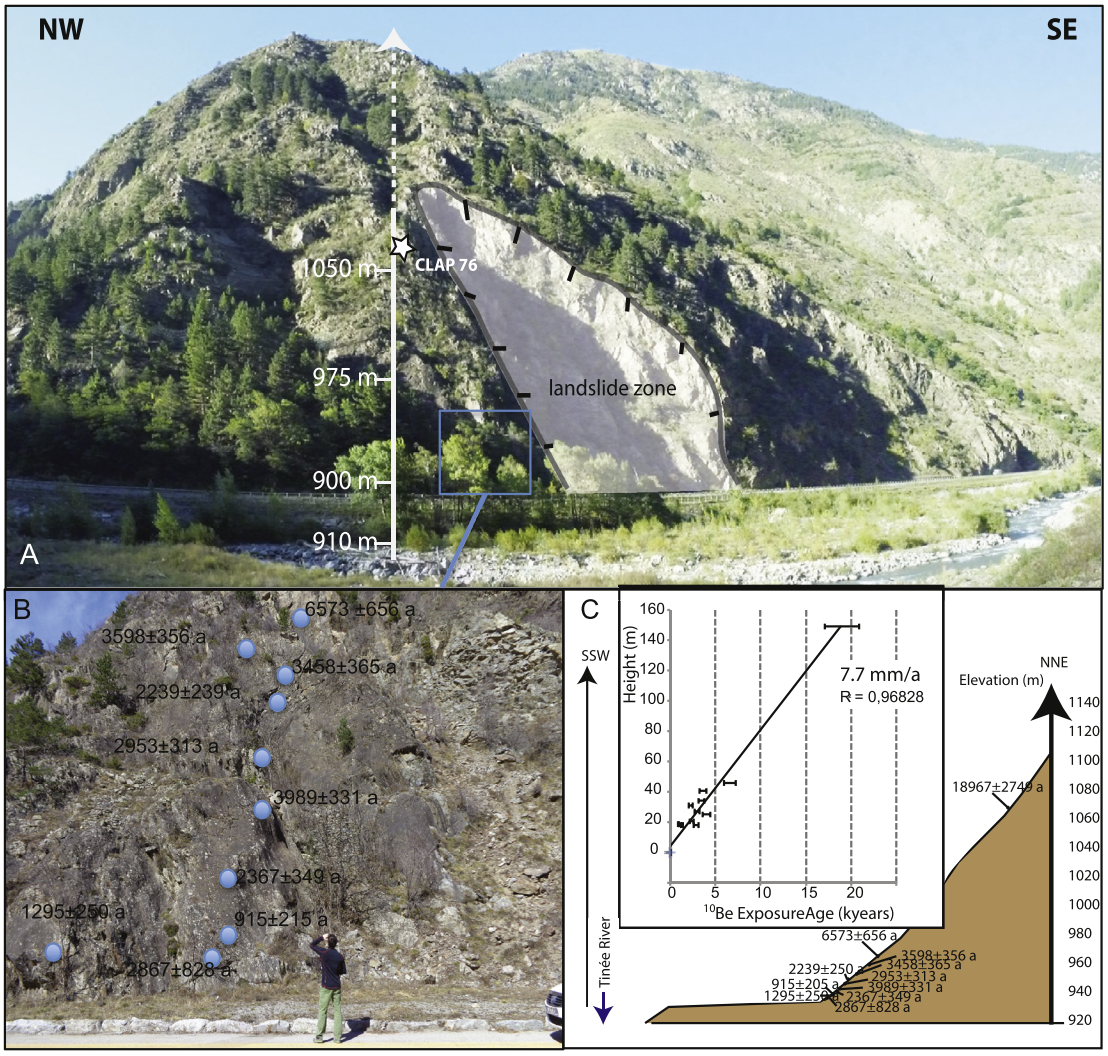

Fig. 4. A, General view of the Isola Gorge. B, detail of the sampled polished river surface. C, CRE ^{10}Be dating results.

Due to the similar (within error) ages in each group, apparent incision rates are very high (>14 mm a^{-1} for group 1 and >5 mm a^{-1} for group 2), separated by a stage of slow incision (<0.2 mm a^{-1}).

4.4. ^{36}Cl dating of the Lower Tinée gorge profile (profile 4)

Fourteen limestone samples of the Lower Tinée Gorge were dated with the ^{36}Cl CRE dating method (Table 2). These ages range between 8.7 ± 0.2 ka at the base of profile and 16.7 ± 0.4 ka at 26 m. The corresponding mean incision rate for the gorge lower 25 m is thus of 1.9 mm a^{-1}. However, except for the highest sample, all ^{36}Cl CRE ages fall into two groups suggesting rapid apparent incision rates:

(i) From 10 to 25 m, CRE ages cluster around 13.3 ± 0.6 ka.
(ii) From 0 to 10 m, CRE ages cluster around 8.6 ± 0.4 ka.

In conclusion, the CRE dating of River polished surfaces shows that 25–150 m of vertical incision occurred along the Tinée River within the last 20 ka, with CRE age groups clustering between (from top to bottom): 1.5–0 ka (Salso Moreno), 2.2–3.5 ka (Isola), 18.1–3 ka (Saint-Sauveur), 13.3–8.6 ka (Lower Tinée). These latter Lower Tinée results are consistent with those obtained in the neighboring Lower Vésubie valley (Saillard et al., 2014).

5. Interpretation and discussion

It is widely thought that river profiles are close to equilibrium conditions, which allows quantifying uplift knowing incision or vice-versa (e.g., Hack, 1960; Molnar and England, 1990; Burbank et al., 1996; Whipple, 2001; Whipple and Tucker, 2002). Considering the orogenic landscapes that are reported to have reached their equilibrium shapes with erosion balancing rock uplift (e.g. Burbank et al., 1996; Pazzaglia and Knuepfer, 2001), this hypothesis may be true over large time periods exceeding a million of years. Such interpretation has led to several major geomorphologic assumptions: (i) river incision rates can be used to estimate long-term regional denudation rates (e.g., Tucker and Slingerland, 1996; Willett, 1999), and (ii) incision and rock uplift balance each other at all time scales (e.g. Snyder et al., 2000; Whipple, 2001). Nevertheless, this general interpretation fails to explain the detailed analyses of incision rates (e.g., Pratt et al., 2002; Rong Yang et al., 2016). In the European Alps, relief shaping is mainly attributed to phases of glaciation driven by global climate cooling events (e.g., discussion in Herman and Champagnac, 2016). However, relationships between glacier advance, retreat and river dynamics in the formation of mountain gorges are still debated (Montgomery and Korup, 2011; Dixon, 2011; Pratt et al., 2002). In the following section, we discuss the possible links between these factors and try to explain the cause of the observed high gorge incision rates.

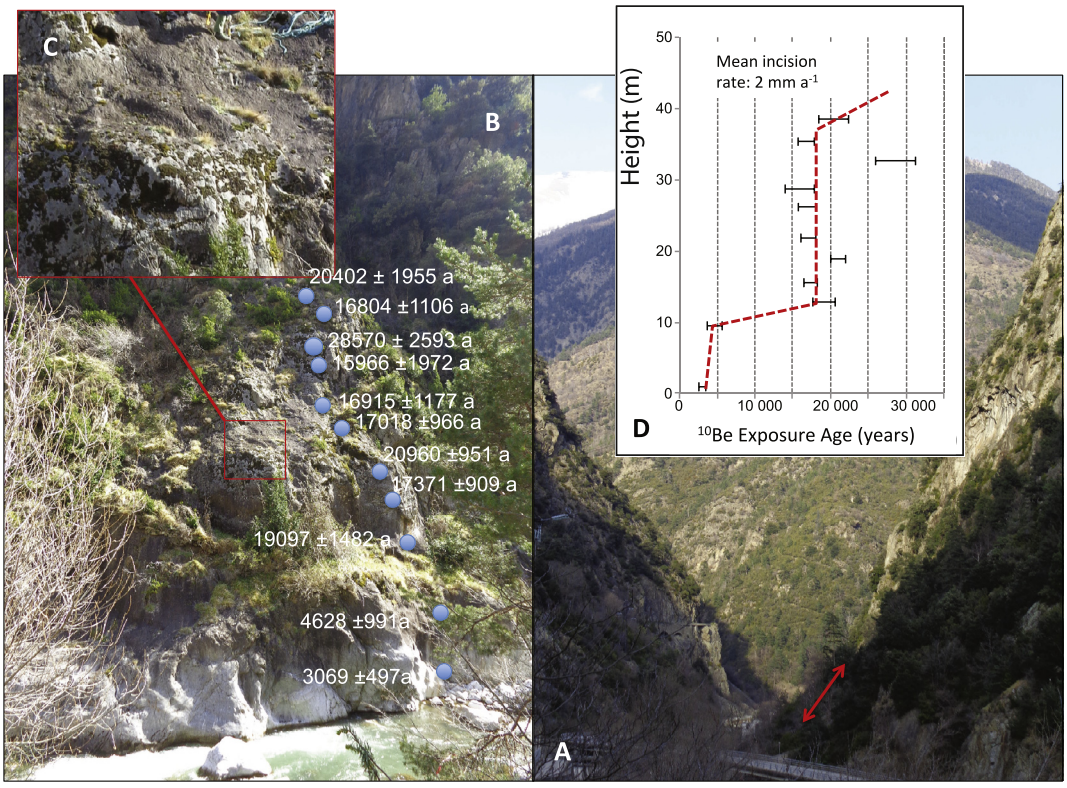

Fig. 5. A, general view towards the north of the Gorge upstream Saint-Sauveur–Sur-Tinée, with the location of the studied scarp. B, Photo of the dated cliff with the corresponding CRE ^{10}Be ages. C, detailed photo showing the polished surface of the scarp. D, CRE ^{10}Be ages versus Height diagram.

5.1. Evidence for high and variable incision rates since 20 ka

According to this study, mean incision rates obtained in the inner gorges of SW French Alps are highly variable (Fig. 7). They vary by a factor >4 (i.e. from 1 to >4 mm a^{-1}), ranging between 1.6 mm a^{-1} in the lower valley and 3–7.7 mm a^{-1} in the higher valley.

The lower bound of these incision rates is a little larger than vertical uplift GPS measurements in Southern French Alps ($\leq$1 mm a^{-1}) (Serpelloni et al., 2013), while the upper bound of these Holocene-scale average estimates is much larger. It is therefore likely that on short timescales, dynamic river equilibrium is not achieved everywhere, at least in the valley upper parts (e.g., Pratt et al., 2002), which in our case is influenced by glaciers. Furthermore, our results clearly show that incision is a transient process, as the dated gorge river-polished surfaces exhibit similar within-error age groups for 10 to 20 m cliff sections (see section 4).

5.2. Potential causes of the high apparent incision rates

These new data acquired in the SW part of the Alpine range are consistent with data collected in other parts of the mountain belt (Brocard et al., 2003; Valla et al., 2010; Montgomery and Korup, 2011), which all show rapid 'apparent' incision rates. In the Tinée Valley, incision of all polished river profiles started at ~20 ka, except for the Upper Salso Moreno profile, which is post 11 ka. This indicates an onset of exhumation of these surfaces at the end of the LGM (20 ka) or of the Younger Dryas (11–12 ka), respectively, and a direct causal link between deglaciation and river bedrock incision. Several hypotheses can be put forward to explain these age clusters and the corresponding high incision rates estimates:

(i) The CRE ages may correspond to a 'true' incision age of the river digging its way down into basement rocks (e.g., Valla et al., 2010). In this case the age clusters reflect phases of extremely rapid incision, linked with an increase of water runoff and/or sediment load, and are spaced by periods of aggradation or stagnation of the river bed (Whipple, 2001; Whipple and Tucker, 2002; Pratt et al., 2002). This effect can be enhanced by the narrowing of the river channel at the onset of faster incision (as observed by the development of wineglass canyons), which focuses incision even more.

(ii) The CRE age clusters may correspond to phases of rapid sediment wash out following phases of burial of the lower valley due to natural dams provided by landslides or frontal moraines (e.g., Pratt et al., 2002). In this case the apparent incision ages may correspond to a rapid rejuvenation of river surfaces during the sediment wash out.

(iii) Finally, the CRE age clusters may correspond to sub-glacial surfaces exposed when the glacier receded, leading to a contemporaneous exposure of a whole scarp that was previously dug below the flowing glacier (e.g., Montgomery and Korup, 2011; Dixon, 2011).

Although it is still difficult to definitively discriminate between these different hypotheses, as the processes may also combine with each other, several lines of evidence distributed among the upper (>1000 m a.s.l.) and lower (0–1000 m a.s.l.) valley parts are highlighted. These two zones clearly show different ages versus incision height patterns, which are tentatively related to their glacial/non-glacial influence (Fig. 7).

5.2.1. In the upper valley part

The valley upper part was either covered by valley glaciers or under their direct influence, as highlighted by reworked moraine remains and polished glacier surfaces at altitudes >1500 m (Darnault et al., 2012; Fig. 2). In the case of the Salso Moreno Gorge, the high incision rate phase occurs a long time (~3–4 ka)

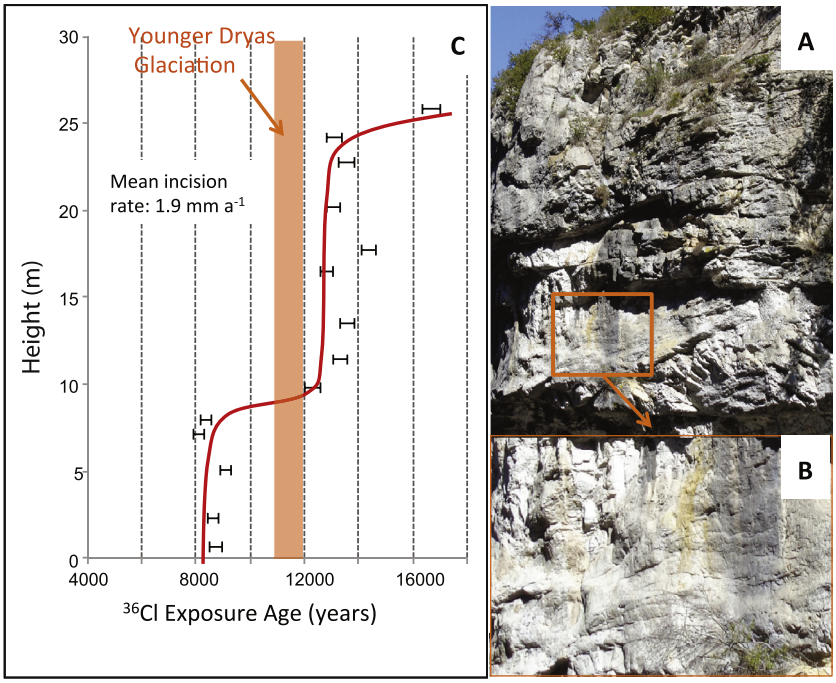

Fig. 6. A, Photograph of the Lower Tinée Gorge. B, detailed photo showing the polished surface of the scarp. C, CRE ^{36}Cl ages versus Height diagram.

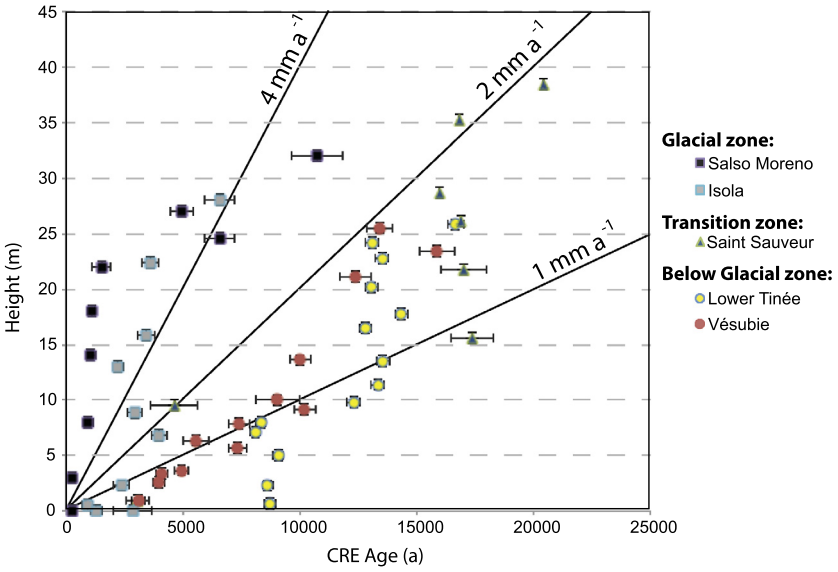

Fig. 7. Synthesis of obtained CRE ages on Inner Gorges profiles. The Vésubie data (orange circles) is from Saillard et al. (2014). (For interpretation of the references to color in this figure, the reader is referred to the web version of this article.)

after deglaciation and is still currently active, which excludes a simple shielding effect of the glacier hiding a sub-glacial gorge. In the Isola gorge, characterized by the highest calculated incision rates (7.7 mm a^{-1}), we obtain (excluding the oldest 20 ka sample) a profile similar to the Salso Moreno one but with a rapid incision starting around 5 ka ago (~5–6 ka after deglaciation). Along the Saint-Sauveur profile, the 18 ± 2 ka age cluster is compatible with all hypotheses (sub-glacial gorge incision, frontal moraine debutressing or efficient incision during deglaciation). These different patterns obtained in relatively close-by areas along the main river stream suggest a discontinuous response of the valley to incision, linked to morphology inheritance from the glacial phases. In the Salso Moreno Gorge, the river directly incises a glacial bar located at the tip of the 2000-m high glacier plateau. It is thus clearly shortcutting a stepped river profile between the high massif which hosted large glaciers during the younger Dryas (11–12 ka; Darnault et al., 2012), and the lower valley, which was glacier-free probably since 18 ka (Brisset et al., 2015). The Saint-Sauveur Gorge lies at the limit of the influence of glaciers, which corresponds to a large step in the river profile (Fig. 1C). Its CRE age versus gorge height pattern appears to be more like the lower, below glacial, valley zone (Fig. 7). It is assumed that the rim of this glacier step was freed from any ice since the onset of deglaciation after the LGM phase and therefore that the river more rapidly dug to its equilibrium profile, while the Isola Gorge lying in the center of this flat zone underwent delayed and on-going incision until the present-day. These data are thus in agreement with Brocard and Van der Beek (2006) who proposed that variations in incision rates are driven by variations in the amount of disequilibrium introduced in the river profiles during the last glaciations. Equilibrium is prob-

ably never reached before the onset of the following glaciation, and thus disequilibrium accumulates from one glacial cycle to the other.

5.2.2. In the low valley part

In both the lower Tinée and Vésubie gorges, incision begun at 16–18 ka (Fig. 7). In the lower Tinée Gorge, a pause in incision clearly occurred during the Younger Dryas glacial phase (Fig. 6). This pause is followed in the two gorges by increased incision occurring just after ∼11 ka in the lower Vésubie (Saillard et al., 2014) and ∼8–9 ka in the lower Tinée (Fig. 7). Finally, regained denudation occurred at c. 4 ka in both the lower Vésubie (Saillard et al., 2014) and Saint-Sauveur gorges, while it is not recorded in the lower Tinée profile. Despite similar elevations, the Tinée profile is thought to stand much farther from the front of glaciers than the Vésubie profile (Fig. 2 in Suppl. Mat. 1). Therefore, in the Vésubie River profile a significant disequilibrium may be inherited from the glacial stage, while the Tinée Profile was already in equilibrium. In this context, the deduced high river incision rates seem to be a response to climatic changes, and most probably to an increase in water runoff. The quiescence of incision during the glacial phases and regained denudation, directly after, are in agreement with increases in sedimentary fluxes during the transitions between glacial and inter-glacial periods (Herman and Champagnac, 2016). Considering the 4 ka phase, it corresponds to the Holocene climatic optimum emphasized through the study of pollens by Peaon et al. (1998), who showed the occurrence of wetter conditions from 3950 to 3850 cal. BP.

5.3. Insights on the formation of inner gorges

The river profiles dated in this study are in agreement with transient, short-lived phases of efficient gorge incision mainly at the onset of inter-glacial periods. Our results confirm that an average incision rate >10 mm a^{-1} is required to shape inner gorges (e.g., Montgomery and Korup, 2011; McPhillips et al., 2016). This value is significantly higher than the long-term incision rate estimated at 0.8 mm a^{-1} for the Alps (Brocard et al., 2003). Such high incision rates are ascribed: (1) to climate variability over several hundred to several thousands of years timescales; (2) to focused erosion in the valleys, the local denudation rate being locally an order of magnitude above the regional denudation rate (Sanchez et al., 2011). Local effects include: (i) the sediment load parameter, very high in the zones of high-incision rates like Salso Moreno Gorge where the moraines are remobilized upstream; (ii) the effect of landslides, triggered by the river base level drop (Bouissou et al., 2012), contributes to the sediment upload in La Clapière upstream the Isola Gorge and (iii) a more focused incision due to channel width reduction. These erosional effects on the particle load might also contribute to the high incision rates obtained in these two latter gorges.

6. Conclusion

The study of mountain gorges in the SW Alps by ^{10}Be and ^{36}Cl CRE dating methods evidences their formation due to non-equilibrium processes during phases of intense and transient incision, spaced by phases of low incision. The incision phases are mainly pulsed during the LGM and Younger Dryas deglacial phases, and the Holocene climatic optimum, which strongly suggests a major coupling of incision with climate fluctuations. However, some CRE ages argue for an on-going rapid incision, especially in the high valley flat parts, previously dug during repeated glaciations.

These zones, where the rivers will tend to shortcut the staircase shaped river profile, are the locus of the most intense incision. For these reasons, the mean incision rates in high-mountain and low-elevation inner gorges are significantly higher (1.6–7.7 mm a^{-1} during the last 20 ka) than the long-term uplift rates of the Alps (c. 1 mm a^{-1}).

Acknowledgements

This work was supported by INSU project 'CALIFE', internal grants from Geoazur Laboratory and Observatoire de la Côte d'Azur. The ASTER AMS national facility (CEREGE, Aix en Provence) is supported by the INSU/CNRS, the ANR through the "Projets thématiques d'excellence" program for the "Equipements d'excellence" ASTER-CEREGE action, IRD and CEA. Authors are grateful to Romain Delunel and An Yin for their constructive reviews and helpful comments, which significantly helped enhance this article.

Appendix A. Supplementary material

Supplementary material related to this article can be found online at http://dx.doi.org/10.1016/j.epsl.2016.10.007.

References

Bauve, V., Plateaux, R., Rolland, Y., Sanchez, G., Bethoux, N., Delouis, B., Darnault, R., 2014. Long-lasting transcurrent tectonics in SW Alps evidenced by Neogene to present-day stress fields. Tectonophysics 621, 85–100. http://dx.doi.org/10.1016/j.tecto.2014.02.006.

Bouissou, S., Darnault, R., Chemenda, A., Rolland, Y., 2012. Evolution of gravity-driven rock slope failure and associated fracturing: geological analysis and numerical modelling. Tectonophysics 526–529, 157–166.

Braucher, R., Merchel, S., Borgomano, J., Bourlès, D.L., 2011. Production of cosmogenic radionuclides at great depth: a multielement approach. Earth Planet. Sci. Lett. 309, 1–9.

Brisset, E., Guiter, F., Miramont, C., Revel, M., Anthony, E.J., Delhon, C., Arnaud, F., Malet, E., de Beaulieu, J.-L., 2015. Lateglacial/Holocene environmental changes in the Mediterranean Alps inferred from lacustrine sediments. Quat. Sci. Rev. 110, 49–71. http://dx.doi.org/10.1016/j.quascirev.2014.12.004.

Brocard, G.Y., Van der Beek, P.A., 2006. Influence of incision rate, rock strength, and bedload supply on bedrock river gradients and valley-flat widths: field-based evidence and calibrations from western Alpine rivers (southeast France). Spec. Pap., Geol. Soc. Am. 398, 101–126.

Brocard, G.Y., Van der Beek, P.A., Bourlès, D.L., Siame, L.L., Mugnier, J.L., 2003. Long-term fluvial incision rates and postglacial river relaxation time in the French Western Alps from ^{10}Be dating of alluvial terraces with assessment of inheritance soil development and wind ablation effects. Earth Planet. Sci. Lett. 209, 197–214.

Burbank, D.W., Leland, J., Fielding, E., Anderson, R.S., Brozovic, N., Reid, M.R., Duncan, C., 1996. Bedrock incision, rock uplift and threshold hillslopes in the northwestern Himalayas. Nature 379 (6565), 505–510.

Chmeleff, J., Von Blanckenburg, F., Kossert, K., Jakob, D., 2010. Determination of the ^{10}Be half-life by multicollector ICP-MS and liquid scintillation counting. Nucl. Instrum. Methods Phys. Res., Sect. B 268, 192–199.

Cossart, E., Fort, M., Bourlès, D., Carcaillet, J., Perrier, R., Siame, L., Braucher, R., 2010. Climatic significance of glacier retreat and rockglaciers re-assessed in the light of cosmogenic dating and weathering rind thickness in Clarée Valley (Briançonnais, French Alps). Catena 80, 204–219.

Darnault, R., Rolland, Y., Braucher, R., Bourlès, D., Revel, M., Sanchez, G., Bouissou, S., 2012. Timing of the last deglaciation revealed by receding glaciers at the Alpine-scale: impact on mountain geomorphology. Quat. Sci. Rev. 31, 127–142.

Delunel, R., Van Der Beek, P.A., Carcaillet, J., Bourlès, D.L., Valla, P.G., 2010. Frost-cracking control on catchment denudation rates: insights from in situ produced ^{10}Be concentrations in stream sediments (Ecrins–Pelvoux massif, French Western Alps. Earth Planet. Sci. Lett. 293 (1), 72–83.

Dixon, J.D., 2011. Deceptively old Alpine gorges. Nat. Geosci. 4, 8–9.

Dunai, T.J., 2001. Influence of secular variation of the geomagnetic field on production rates of in situ produced cosmogenic nuclides. Earth Planet. Sci. Lett. 193 (1), 197–212.

Dunai, T., Stuart, F.M., 2009. Reporting of cosmogenic nuclide data for exposure age and erosion rate determinations. Quat. Geochronol. 4, 437–440.

Dunne, J., Elmore, D., Muzikar, P., 1999. Scaling factors for the rates of production of cosmogenic nuclides for geometric shielding and attenuation at depth on sloped surfaces. Geomorphology 27, 3–11.

Federici, P.R., Granger, D.E., Pappalardo, M., Ribolini, A., Spagnolo, M., Ca, A.J., 2008. Exposure age dating and equilibrium line altitude reconstruction of an Egesen moraine in the Maritime Alps, Italy. Boreas 37, 245–253.

Gosse, J.C., Phillips, F.M., 2001. Terrestrial in situ cosmogenic nuclides: theory and application. Quat. Sci. Rev. 20, 1475–1560.

Hack, J.T., 1960. Interpretation of erosional topography in humid temperate regions. Am. J. Sci. 258-A, 80–97.
Herman, F., Champagnac, J.D., 2016. Plio-Pleistocene increase in erosion rates in mountain belts in response to climate change. Terra Nova 28 (1), 2–10. http://dx.doi.org/10.1111/ter.12186.
Ivy-Ochs, S., Kerschner, H., Maisch, M., Christl, M., Kubik, P.W., Schlüchter, C., 2009. Latest Pleistocene and Holocene glacier variations in the European Alps. Quat. Sci. Rev. 28, 2137–2149.
Jourdon, A., Rolland, Y., Petit, C., Bellahsen, N., 2014. Style of Alpine tectonic deformation in the Castellane fold-and-thrust belt (SW Alps, France): insights from balanced cross-sections. Tectonophysics 633, 143–155.
Kelsey, H.M., 1988. Formation of inner gorges. Catena 15, 433–458.
Koppes, M.N., Montgomery, D.R., 2009. The relative efficacy of fluvial and glacial erosion over modern to orogenic timescales. Nat. Geosci. 2, 644–647.
Korschinek, G., Bergmaier, A., Faestermann, T., Gerstmann, U.C., et al., 2010. A new value for the half-life of ^{10}Be by heavy-ion elastic recoil detection and liquid scintillation counting. Nuclear Instruments and Methods in Physics Research B, 187–191.
McEwen, L.J., Matthews, J.A., Shakesby, R.A., Berrisford, M.S., 2002. Holocene gorge excavation linked to boulder fan formation and frost weathering in a Norwegian alpine periglaciofluvial system. Arct. Antarct. Alp. Res. 34, 346–358.
McPhillips, D., Hoke, G.D., Liu-Zeng, J., Bierman, P.R., Rood, D.H., Niedermann, S., 2016. Dating the incision of the Yangtze River gorge at the First Bend using three-nuclide burial ages. Geophys. Res. Lett. 43, 101–110. http://dx.doi.org/10.1002/2015GL066780.
Meigs, A., Krugh, W.C., Davis, K., Bank, G., 2006. Ultra-rapid landscape response and sediment yield following glacier retreat, Icy Bay, southern Alaska. Geomorphology 78, 207–221.
Merchel, S., Arnold, M., Aumaître, G., Benedetti, L., Bourlès, D.L., Braucher, R., Alfimov, V., Freeman, S.P.H.T., Steier, P., Wallner, A., 2008. Towards more precise ^{10}Be and ^{36}Cl data from measurements at the 10^{-14} level: influence of sample preparation. Nucl. Instrum. Methods Phys. Res., Sect. B, Beam Interact. Mater. Atoms 266, 4921–4926.
Molnar, P., England, P.C., 1990. Late Cenozoic uplift of mountain ranges and global climate change: chicken or egg? Nature 346, 29–34.
Montgomery, D.R., Korup, O., 2011. Preservation of inner gorges through repeated Alpine glaciations. Nat. Geosci. 4 (1), 62–67.
Nishiizumi, K., Imamura, M., Caffee, M.W., Southon, J.R., Finkel, R.C., McAninch, J., 2007. Absolute calibration of ^{10}Be AMS standards. Nucl. Instrum. Methods Phys. Res., Sect. B, Beam Interact. Mater. Atoms 258, 403–413.
Ouimet, W.B., Whipple, K.X., Crosby, B.T., Johnson, J.P., Schildgen, T.F., 2008. Epigenetic gorges in fluvial landscapes. Earth Surf. Process. Landf. 33, 1993–2009.
Pazzaglia, F.J., Knuepfer, P.L.K., 2001. The Steady-State Orogen: Concepts, Field Observations, and Models. Kline Geology Laboratory, Yale University.
Peaon, O., Guiot, J., Cheddadi, R., Tarasov, P., Reille, M., de Beaulieu, J.L., Bottema, S., Andrieu, V., 1998. Climatic reconstruction in Europe for 18 000 a BP from pollen data. Quat. Res. 49, 183–196.
Penck, A., Brückner, E., 1909. Die Alpen im Eiszeitalter, vol. 3. Tauchnitz, Leipzig. 1199 pp.
Pratt, B., Burbank, D.W., Heimsath, A., Ojha, T., 2002. Impulsive alluviation during early Holocene strengthened monsoons, central Nepal Himalaya. Geology 30, 911–914.
Rong, Yang, Fellin, M.G., Herman, F., Willett, S.D., Wei, Wang, Maden, C., 2016. Spatial and temporal pattern of erosion in the Three Rivers Region, southeastern Tibet. Earth Planet. Sci. Lett. 433, 10–20.
Saillard, M., Petit, C., Rolland, Y., Braucher, R., Bourlès, D.L., Zerathe, S., Revel, M., Jourdon, A., 2014. Late Quaternary incision rates in the Vésubie Catchment area (Southern French Alps) from in situ-produced ^{36}Cl cosmogenic nuclide dating: Tectonic and climatic implications. J. Geophys. Res., Earth Surf. 119 (5), 1121–1135.
Sanchez, G., Rolland, Y., Corsini, M., Braucher, R., Bourlès, D., Arnold, M., Aumaître, G., 2010. Relationships between tectonics, slope instability and climate change: cosmic ray exposure dating of active faults, landslides and glacial surfaces in the SW Alps. Geomorphology 117, 1–13.
Sanchez, G., Rolland, Y., Corsini, M., Jolivet, M., Brichaud, S., Carter, A., 2011. Exhumation controlled by transcurrent tectonics: the Argentera-Mercantour massif (SW Alps). Terra Nova 23, 116–126.
Schimmelpfennig, I., Benedetti, L., Finkel, R., Pik, R., Blard, P.-H., Bourlès, D., Burnard, P., Williams, A., 2009. Source of in situ ^{36}Cl in basaltics rocks. Implication for calibration of production rates. Quat. Geochronol. 4, 441–461.
Schlunegger, F., Hinderer, M., 2003. Pleistocene/Holocene climate change, re-establishment of fluvial drainage network and increase in relief in the Swiss Alps. Terra Nova 15, 88–95.
Serpelloni, E., Faccenna, C., Spada, G., Dong, D., Williams, S.D., 2013. Vertical GPS ground motion rates in the Euro-Mediterranean region: new evidence of velocity gradients at different spatial scales along the Nubia–Eurasia plate boundary. J. Geophys. Res. B, Solid Earth Planets 118 (11), 6003–6024.
Snyder, N.P., Whipple, K.X., Tucker, G.E., Merritts, D.J., 2000. Landscape response to tectonic forcing; digital elevation model analysis of stream profiles in the Mendocino triple junction region, Northern California. Geol. Soc. Am. Bull. 112 (8), 1250–1263.
Stone, J.O., 2000. Air pressure and cosmogenic isotope production. J. Geophys. Res. 105, 753–760.
Tucker, G.E., Slingerland, R., 1996. Predicting sediment flux from fold and thrust belts. Basin Res. 8, 329–349.
Valla, P.G., Van der Beek, P.A., Carcaillet, J., 2010. Dating bedrock gorge incision in the French Western Alps (Ecrins–Pelvoux massif) using cosmogenic ^{10}Be. Terra Nova 22, 18–25.
Valla, P.G., Shuster, D.L., Van der Beek, P.A., 2011. Significant increase in relief of the European Alps during mid-Pleistocene glaciations. Nat. Geosci. 4, 688–692.
Vernon, A.J., Van der Beek, P.A., Sinclair, H.D., Rahn, M.K., 2008. Increase in late Neogene denudation of the European Alps confirmed by analysis of a fission-track thermochronology database. Earth Planet. Sci. Lett. 270, 316–329.
Whipple, K.X., 2001. Fluvial landscape response time: how plausible is steadystate denudation? Am. J. Sci. 301, 313–325.
Whipple, K.X., Tucker, G.E., 2002. Implications of sediment-flux-dependent river incision models for landscape evolution. J. Geophys. Res., Solid Earth (1978–2012) 107 (B2), ETG-3.
Willett, S.D., 1999. Orogeny and orography; the effects of erosion on the structure of mountain belts. J. Geophys. Res. B, Solid Earth Planets 104 (12), 28957–28982.